Advances in Science and Technology
Research Journal
Volume 10, No. 29, March 2016, pages 71–84
DOI: 10.12913/22998624/61935

Research Article

MATERIAL SIGNATURE ORTHONORMAL MAPPING IN HYPERSPECTRAL UNMIXING TO ADDRESS ENDMEMBER VARIABILITY

Ali Jafari[1], Mohammad Mehdi Ebadzadeh[1], Reza Safabakhsh[1]

[1] Computer and Information Technology Engineering Department, Amirkabir University of Technology, 424 Hafez Ave, Tehran, Iran, e-mail: ebadzadeh@aut.ac.ir

Received: 2015.12.15
Accepted: 2016.02.01
Published: 2016.03.01

ABSTRACT

A new hyperspectral unmixing algorithm which considers endmember variability is presented. In the proposed algorithm, the endmembers are represented by correlated random vectors using the stochastic mixing model. Currently, there is no published theory for selecting the appropriate distribution for endmembers. The proposed algorithm first uses a linear transformation called material signature orthonormal mapping (MSOM), which transforms the endmembers to correlated Gaussian random vectors. The MSOM transformation reduces computational requirements by reducing the dimension and improves discrimination of endmembers by orthonormalizing the endmember mean vectors. In the original spectral space, the automated endmember bundles (AEB) method extracts a set of spectra (endmember set) for each material. The mean vector and covariance matrix of each endmember estimated directly from endmember sets in the MSOM space. Second, a new maximum likelihood method, called NCM_ML, is proposed which estimates abundances in the MSOM space using the normal compositional model (NCM). The proposed algorithm is evaluated and compared with other state-of-the-art unmixing algorithms using simulated and real hyperspectral images. Experimental results demonstrate that the proposed unmixing algorithm can unmix pixels composed of similar endmembers in hyperspectral images in the presence of spectral variability more accurately than previous methods.

Keywords: abundance, endmember variability, Hyperspectral unmixing, normal compositional model (NCM), spectral mixture analysis (SMA), stochastic mixture model (SMM).

INTRODUCTION

Hyperspectral imaging sensors collect images from the surface over many contiguous bands of high spectral resolution [1]. These images have many applications in various fields including agriculture, resource management, geography, geology, land-use monitoring, and mineral identification [2, 3]. Pixels of hyperspectral image are assumed to be mixtures of a few materials, due to low spatial resolution of a sensor, microscopic material mixing, and multiple scattering [4].

In the macroscopic mixing scale, it is assumed that the pixel spectra are weighted linear combinations of the present material spectra (endmembers) [5, 6]. This is called a linear mixture model (LMM). The individual spectra weights are introduced as material abundance fractions within the spatial extent of the pixel on the ground. More precisely, according to the LMM, each pixel of a hyperspectral image (p_i for i = 1,…, N) is assumed to be a mixture of *M* spectra *Em*, where *m* = 1,…, *M* as in the following equation:

$$p_i = [p_{i1} \quad \dots \quad p_{iL}]^T = \sum_{m=1}^{M} f_{mi}\, E_m + \varepsilon_i \quad (1)$$

where: $E_m = [E_{m1} \quad \dots \quad E_{mL}]^T$ is the spectrum of the m^{th} material,
f_{mi} – is the abundance fraction of the m^{th} material in the i^{th} pixel,
ε_i – is an error term,
N – is the number of pixels,
L – is the number of spectral bands.

Due to physical considerations [6], two constraints are generally imposed into the model described in (1): the abundance non-negativity constraint, since negative endmember contributions are physically unrealistic, and the abundance sum-to-one constraint, which indicates that the endmember contribution must add up to 100%, as follows:

$$f_{mi} \geq 0 \quad (2)$$

$$\sum_{m=1}^{M} f_{mi} = 1. \quad (3)$$

Endmember extraction is identifying the spectra of the pure ground components or endmembers [16, 21, 27]. After endmember extraction, spectral unmixing is used to estimate the endmember abundances in each pixel. In literature, performing endmember extraction and abundance estimation is called spectral mixture analysis (SMA) [16, 21]. Several automatic endmember extraction algorithms have been developed for extraction of spectral endmembers from hyperspectral image data. The algorithms in this category include the pixel purity index (PPI), N-finder, iterative error analysis, automated morphological endmember extraction algorithm, convex cone analysis, minimum volume transform, and vertex component analysis among many others [21]. In the LMM, the abundance estimation is a linear inversion problem. Many approaches, such as constrained least squares and minimum variance estimators are used to solve this problem [9].

The basic assumption of LMM is that every pure material in a given scene is represented by a constant spectral signature [6]. However, the spectra of a pure material in a given scene can have variations [8, 1, 21]. In other words, endmembers are not constant signatures in any given scene. Endmember variability occurs for a number of reasons, including environmental, atmospheric, and intrinsic factors [28]. The assumption of a constant spectral signature for endmembers in LMM may reduce the accuracy of spectral unmixing in abundance estimations [20]. It is the most important source of abundance estimation errors in conventional unmixing methods [20, 23].

An alternative to LMM is the stochastic mixing model, which represents each endmember as a random vector [12]. In this model, each sample from the random vector can represent a possible spectral signature of the corresponding material. In the stochastic mixing model, the hyperspectral pixels are random vectors distributed according to a1 linear combination of endmembers. In this approach, it is possible to cover endmember variability by defining the proper distribution for random vectors representing endmembers. Defining proper distribution requires exact knowledge of endmember variability, which may not be easy to obtain in practice. Diverse methods of hyperspectral unmixing have assumed different statistical distributions for endmember random vectors. Depending on the assumed distribution, this approach may result in representations that cannot represent the full variation of endmembers or allow for endmember variations that are not physically meaningful [28]. In particular, gamma, beta and normal distributions have been assumed for endmember representations [28], which are called the beta compositional model (BCM), gamma compositional model (GCM) and normal compositional model (NCM). Currently, there is no published theory for selecting the appropriate distribution for endmembers. Previously, the majority of hyperspectral unmixing methods have used the NCM [22, 12].

There is a high degree of similarity among the spectra of various endmembers [25]. Similarity among endmembers reduces discrimination among different endmembers and reduces the accuracy of spectral unmixing in abundance estimations [20].

This paper proposes an improved SMA technique based on a new linear transformation called material signature orthonormal mapping (MSOM), along with a new maximum likelihood technique, to address endmember variability. The proposed unmixing algorithm uses the stochastic mixing model. To choose a proper distribution for endmembers, a linear combination of different hyperspectral bands is considered. According to the *central limit theorem*, the sum of non-Gaussian random variables is closer to the Gaussian random variable than the original [14, 13]. Thus any linear combination of hyperspectral bands is closer to the Gaussian random variable than the original bands. The proposed algorithm uses a linear transformation called material signature orthonormal mapping (MSOM), which orthonormalizes the endmember mean vectors and reduces the dimensionality of the data (endmember and pixel vectors) from *L* (number of spectral bands) to *M* (number of spectral endmembers). The MSOM transformation performs a linear mapping of the original hyperspectral bands to a new space. The generated features in the MSOM space are closer to the Gaussian distribution than the original features. Due to the large number of bands

in hyperspectral data, the features in the MSOM space have an approximately normal distribution. Thus, in the MSOM space, the endmembers are represented by correlated Gaussian random vectors. The proposed unmixing algorithm uses the automated endmember bundles (AEB) method to extract a set of spectra to represent each material. The mean vector and covariance matrix of each endmember estimated directly from endmember sets in the MSOM space. Finally, a new maximum likelihood method, called NCM_ML, is proposed, which estimates abundances in the MSOM space using NCM.

In the following, Section II reviews the AEB [21], and the related work. Section III presents the proposed algorithm for abundance estimation. Results are shown in Section IV. Conclusions are given in Section V.

BACKGROUND

Automated Endmember Bundles

AEB [21] is an endmember set extraction method from hyperspectral image data. AEB uses a standard endmember extraction algorithm, such as vertex component analysis, for endmember set extraction. The main assumption is that there are a lot of pure pixels for each material in the scene, and one can assume that the pure pixels will also be present in the image subsets generated by random sampling.

Thus by applying the vertex component analysis algorithm to a randomly selected subset of the original hyperspectral image, one can obtain a unique set of endmembers. By running endmember extraction on several image subsets, a set of spectra from the different ground components is generated. By using a K-means clustering algorithm, with the Euclidean distance or spectral angle as the similarity measure, the estimated endmembers are divided into separate endmember bundles for each ground component.

Related work

In [28] the unmixing methods that account for endmember variability were organized into two general categories based on the variable endmember representation used: endmembers as sets and endmembers as statistical distributions. The most generally used solution to account for endmember variability is a multiple endmember spectral mixture analysis (MESMA) [18]. A MESMA is an iterative algorithm, which uses a set of spectra to represent each endmember. The algorithm decomposes mixed pixel iteratively using all possible endmember combinations which are selected from endmember sets. The algorithm returns the abundances demonstrating the best fit (i.e., lowest RMSE) spectrum for the pixel. FCLS-MESMA method uses the FCLS method in the decomposing of the pixel.

The majority of hyperspectral unmixing methods have used the normal compositional model (NCM) [22, 12]. The NCM uses the basic combination model of LMM. In the NCM, the hyperspectral pixels are multivariate Gaussian random vectors, distributed according to the linear combination of endmembers as follows:

$$p_i = \sum_{m=1}^{M} f_{mi}\, \boldsymbol{\varepsilon_m}, \tag{4}$$

where: ε_i – are independent Gaussian random vectors representing endmembers.

The abundance non-negativity and sum-to-one constraints are two physical constraints on this model, as they were in the LMM case. The Gaussian random vectors are determined by two parameters: the mean vector and the covariance matrix.

$$\boldsymbol{\varepsilon_m} \sim \mathcal{N}(E_m, C_m), \tag{5}$$

where: E_m – is the $L\times1$ mean vector,
C_m – is the $L\times L$ covariance matrix of the m^{th} endmember.

Different bands in hyperspectral images are often highly correlated, and fully correlated covariance matrices are used to consider these correlations.

Various methods for spectral unmixing and endmember estimation have been developed using the NCM [10, 11, 21, 22, 26, 27]. Most of these methods estimate unknown parameters by maximizing the likelihood function. The likelihood function for each pixel is:

$$f(p_i) = \mathcal{N}\left(\sum_{m=1}^{M} f_{mi}\, E_m,\ \sum_{m=1}^{M} f_{mi}^2\ C_m\right). \tag{6}$$

The joint likelihood for all the pixels is assumed to be the product of the individual likelihoods:

$$f = \prod_{i=1}^{N} f(p_i). \tag{7}$$

where: N – is the number of pixels.

In [22] a method for estimating the parameters of the NCM using a nested stochastic expectation maximization algorithm is presented. In the main expectation maximization loop of the algorithm,

endmember parameters (mean and covariance) are updated assuming the known abundance values, and then abundance values are updated assuming the known endmember parameters. Updating endmember parameters is done by maximizing the joint likelihood function in equation (7) using another expectation maximization algorithm. Updating abundance values assuming the known endmember parameters is done by maximizing the likelihood function defined in equation (6), subject to the abundance non-negativity and sum-to-one constraints.

In [26] a piecewise convex model is proposed, which partitions the input data set into several convex regions. Assuming NCM for each convex region, the proposed endmember distribution detection (ED) algorithm determines endmember distributions and proportion values. The ED algorithm assumed the known covariance matrices for all endmembers and defined appropriate priors on the endmember mean vectors ($f(E)$) and abundance vectors ($f(\{f_i\}_{i=1}^N)$). The ED algorithm iteratively maximizes $f(X|E,P)\,f(E)\,f(\{f_i\}_{i=1}^N)$ where $f(X \mid E,\{f_i\})$ is the joint likelihood defined in equation (7). The algorithm proceeds by iteratively maximizing the log of $f(p_i \mid E,f_i)\,f(f_i)$ to update the abundance vectors, maximizing $f(X \mid E,\{f_i\})\,f(E)$ to update endmember mean vectors and updating the abundance prior parameters. If endmember means and covariances are known, these can be held constant during the ED algorithm while the abundance vectors are estimated.

Most of the methods for spectral unmixing use the Bayesian approach for parameter estimation in NCM. A number of simplified assumptions are considered to reduce estimation complexity. However, these assumptions can reduce algorithm performance.

In [10] a Bayesian unmixing algorithm for the NCM to estimate the abundance coefficients is presented. In this algorithm all endmembers have the same covariance matrix. The covariance matrix is proportional to the identity matrix ($\sigma^2 I$). The unknown parameters (σ and abundances) are estimated in the Bayesian framework. A uniform distribution over the set of all feasible abundance vectors (with abundance non-negativity and sum-to-one constraints) is chosen for the abundance prior. A conjugate inverse Gamma distribution is chosen for the σ^2 prior. A fixed shape parameter for the inverse gamma distribution is considered and the scale parameter is estimated using a hierarchical Bayesian algorithm. In this algorithm a non-informative Jeffrey's prior is assumed for the scale parameter. Using defined priors and the likelihood function defined in equation (7), joint posterior distribution of the unknown parameters can be derived. However the derived posterior distribution is too complex to derive the minimum mean square error or the maximum a posteriori estimators of the unknown parameters. Thus a hybrid Gibbs sampler is proposed to generate samples distributed according to the posterior and to use the generated samples to approximate the Bayesian estimators. The algorithm is extended to the case where endmembers have different variances. Thus, in both methods the covariance matrix is assumed to be proportional to the identity matrix.

The diagonal covariance assumption in the NCM model diminishes model accuracy. Based on the high degree of correlation among different wavelengths, neighboring bands are dependent. Despite the dependency of different bands, using the diagonal covariance matrix, different bands are considered independent. In [15] a Bayesian unmixing algorithm for the NCM was presented that uses a general non-diagonal matrix for endmember covariance matrices. In this algorithm all endmembers share an identical covariance matrix. This algorithm uses hybrid Markov Chain Monte Carlo sampling strategies to estimate abundances.

In [27] the sampling piecewise convex unmixing and endmember extraction (S-PCUE) algorithm proposed. This algorithm uses a piecewise convex model and partitions the input data set into several convex regions. In each convex region, the NCM is used. The S-PCUE uses a complete Bayesian inference strategy to estimate the number of endmember sets needed to represent the hyperspectral image and sets of endmembers and the abundances for each data point. These parameters are attained using a Gibbs sampling approach. All endmember distributions are given the same covariance matrix, which is proportional to the identity matrix. For each partition, the means of the associated endmember distributions are assumed to share a Gaussian prior distribution. Other priors are considered for parameters of this distribution. A Dirichlet distribution is considered for abundance priors.

PROPOSED METHOD

This section proposes a new SMA algorithm to decompose mixed pixels in hyperspectral im-

agery considering endmember variability. Figure 1 summarizes the different steps involved in the proposed unmixing method. This algorithm consists of three steps: first, the AEB extracts a set of spectra from the input image in order to represent each material. Second, a new linear transformation, called MSOM, is proposed which orthonormalizes the endmember mean vectors and reduces the dimensionality of the data. This transformation leads to higher discrimination of endmembers. Then both mixed pixels and endmember sets are mapped onto the MSOM space. In the MSOM space each endmember is represented by a random vector. Due to the large number of bands in the original hyperspectral data, according to the *central limit theorem*, the features in the MSOM space have an approximately normal distribution. Thus, in the MSOM space, the endmembers are represented by correlated Gaussian random vectors. The mean vector and covariance matrix of each endmember estimated directly from endmember sets in the MSOM space. Finally, a new maximum likelihood method, called NCM_ML, is proposed which estimates abundances in the MSOM space using NCM.

Extraction of endmember sets

One approach to account for endmember variability is to represent each present material with a set or "bundle" of spectra [28]. The AEB algorithm is a conceptually straightforward technique to derive endmember sets from a hyperspectral image. In this step, the endmember sets automatically extracted from the input image using the AEB algorithm.

Material signature orthonormal mapping (MSOM)

The second step of the proposed unmixing algorithm is a linear transformation called MSOM. The MSOM maps endmembers and input pixels to a new space called MSOM space. Unmixing is done in the MSOM space. The MSOM transformation can solve three major challenges in hyperspectral unmixing. The first major challenge is defining a proper distribution for endmembers. The proposed unmixing algorithm represents each endmember by a correlated random vector. Defining proper distribution requires exact knowledge of endmember variability, which may not be easy to obtain in practice. The majority of hyperspectral unmixing methods have used the Gaussian distribution for endmember random vectors. The Gaussian distribution is not an appropriate distribution for endmembers in the original space [28]. Due to the large number of bands in hyperspectral data, applying a linear transformation to the hyperspectral data can produce features with an approximately normal distribution. The second major challenge is the high degree of similarity among spectra of different endmembers in a scene. Thus, different endmember spectra are very close to each other in the L-dimensional space, and the angles among different spectra are small [17]. Therefore the endmember matrix tends to become singular and unstable. In this case, spectral unmixing produces a large error term and is sensitive to small changes in the input spectra (endmember variability) and highly sensitive to noise [24]. The third major challenge is the high dimensionality of the hyperspectral data, which causes a high computational cost for hyperspectral analysis [19]. To decrease the computational cost of hyperspectral unmixing, the number of dimensions is usually reduced before hyperspectral unmixing.

In order to address these three challenges, if a linear transformation is defined to simultaneously reduce the dimension and improve the discrimination of endmembers, then this linear transformation can resolve all three challenges. To improve the discrimination of endmembers, signal representation in the lower-dimensional

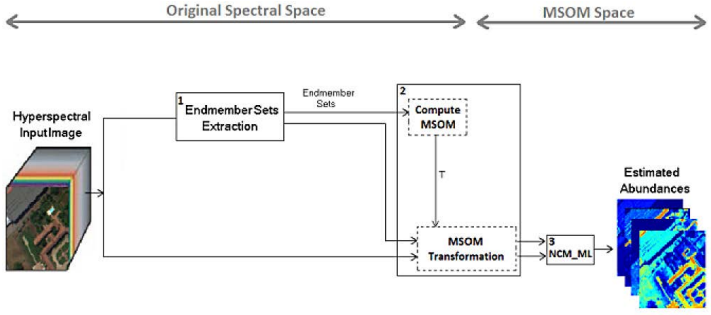

Fig. 1. Block diagram illustrating the proposed method for spectral unmixing considering endmember variability

space must sufficiently retain the requisite information for successful unmixing. Thus, we seek a linear combination of features, which maximally separates diverse materials. To reach this goal, we seek a new lower dimensional space such that each endmember mean vector is orthonormal with other endmember mean vectors. In the lower dimensional space, endmember mean vectors are orthonormal. Consequently, the new space has at least *M* dimensions.

Suppose that *E* is the *L*×*M* endmember matrix, where the i^{th} column of $E(E_i)$ is the mean vector of the i^{th} endmember (as a random vector). Suppose also that *T* is an *M*×*L* transformation matrix and $F = TE$ is an *M*×*M* endmember matrix in the new space. We want to have orthonormal columns in *F*. Thus:

$$F^T F = E^T T^T T E = I, \tag{8}$$

and

$$E E^T T^T T E E^T = E\, E^T. \tag{9}$$

If we take $\mathrm{T} = \Lambda^{-\frac{1}{2}}\Phi$ the above equation is satisfied, where Λ and Φ are the eigen value and vector matrices of the EE^T, ($EE^T = \Phi\, \Lambda\, \Phi^T$). Note that *E* is an *L*×*M* matrix (*M*<*L*). Thus, at most *M* eigenvalues of EE^T are nonzero. We build *T* by taking the *M* nonzero eigenvalues and corresponding eigenvectors of EE^T. Thus, *T* is an *M*×*L* transformation matrix and reduces the dimension of data to *M*.

NCM_ML method

The third step of the proposed unmixing algorithm is abundance estimation. In the MSOM space we assume NCM model and represent each material with a correlated Gaussian random vector. The mean vector and covariance matrix of each endmember estimated directly from endmember sets in the MSOM space. In this step, a new maximum likelihood method, called NCM_ML, is proposed which estimates abundances for each mixed pixel.

Each mixed pixel is a sample from the Gaussian random vector $\boldsymbol{P_i} = \sum_{m=1}^{M} f_{mi}\, \boldsymbol{\mathcal{E}_m}$. Note that the mean vector and covariance matrix of $\boldsymbol{P}_i$ are indicated by $\overline{\boldsymbol{P}}_{\boldsymbol{i}}$ and Σ_{P_i},, respectively. The maximum likelihood estimation of the abundance vector f_i is done by minimizing a cost function based on the Mahalanobis distance between p_i and $\overline{\boldsymbol{P}}_{\boldsymbol{i}}$ [7]:

$$cost = (p_i - \overline{\boldsymbol{P}}_{\boldsymbol{i}})^T\, {\Sigma_{P_i}}^{-1}\, (p_i - \overline{\boldsymbol{P}}_{\boldsymbol{i}}), \tag{23}$$

where: $\Sigma_{P_i} = {f_{1i}}^2\, \Sigma_1 + \cdots + {f_{Mi}}^2\, \Sigma_M$

Consequently,

$$cost = (p_i - E\, f_i)^{\boldsymbol{T}} \left({f_{1i}}^2\, \Sigma_1 + \cdots + {f_{Mi}}^2\, \Sigma_M\right)^{-1} (p_i - E\, f_i). \tag{24}$$

Now, the gradient descent method is used for minimizing the cost function. The gradient of the cost function is calculated as:

$$\frac{\boldsymbol{\partial cost}}{\boldsymbol{\partial} f_{ij}} = -2\, E_i\, {\Sigma_P}^{-1}\, (p_i - E\, f_i) - 2\, f_{ij}(p_i - \cdot$$
$$- E\, f_i)^{\boldsymbol{T}}\, {\Sigma_P}^{-1}\, \Sigma_j\, {\Sigma_P}^{-1}\, (p_i - E\, f_i), \tag{25}$$

$$grad(cost) = \frac{\boldsymbol{\partial cost}}{\boldsymbol{\partial} f_i} = \begin{bmatrix} \frac{\boldsymbol{\partial cost}}{\boldsymbol{\partial} f_{1\mathrm{i}}} \\ \vdots \\ \frac{\boldsymbol{\partial cost}}{\boldsymbol{\partial} f_{Mi}} \end{bmatrix}. \tag{26}$$

We use the penalty method to consider constraints in the optimization. The penalty term for the abundance sum-to-one constraint is defined as:

$$penalty = (\mathbf{1}^T f_i - 1)^2. \tag{29}$$

where: $\mathbf{1} = [(1\ldots1)]^T$ is a *L*×1 vector. The gradient of penalty term is:

$$penalty = (\mathbf{1}^T f_i - 1)^2. \tag{30}$$

For the abundance non-negativity constraint, we used the same approach. However the penalty term is applied when the constraint does not hold. In each iteration, a new abundance vector is determined. If one of the abundances (e.g. $f(\boldsymbol{i})$) has a negative value, the corresponding gradient of the penalty term is added to the gradient vector. The gradient of the penalty term is 1.

RESULTS

The proposed unmixing algorithm is evaluated in this section. Moreover, the proposed algorithm is compared with other abundance estimation methods using simulated and real hyperspectral data. Two different case studies are considered that demonstrate the potential of the proposed methodology in two different analysis scenarios: (a) an urban area at the Pavia University, and (b) an agricultural area at the Indian Pine test site.

The perfect abundances associated with the simulated data allow accurate validation of algorithms in a fully controlled analysis scenario.

Results on the HySens Pavia University data

The proposed algorithm was run on simulated and real hyperspectral data using the Pavia University data set. The Pavia University data set is a 115 band hyperspectral image acquired over the University of Pavia by reflective optics systems

Imaging Spectrometer (ROSIS) on 8 July 2002. The sensor has spectral coverage ranging from 0.43 to 0.86 μm with a bandwidth of 4 nm. This image has spatial resolution of 1.3 meters per pixel. 12 bands are removed due to low signal to noise ratio (SNR) and the remaining 103 spectral bands are used. There is ground truth data for this image. Nine land-cover classes were identified in the University campus: trees, asphalt, bitumen, gravel, painted metal sheets, shadows, self-blocking bricks, meadows, and bare soil. Figure 2a shows a false color composite of this image, while Figure 2b shows the nine ground-truth classes of interest.

Each class of the Pavia University data set was represented by a multivariate Gaussian random endmember. The mean and covariance matrix of each multivariate Gaussian random endmember was estimated from a set of spectra chosen from a corresponding class. Twenty samples from each class of the Pavia University data-set were selected for endmember set construction. The sample mean and sample covariance of each endmember set were used for the determination of the multivariate Gaussian random endmember mean and covariance matrices. The endmember samples are shown in Figure 3.

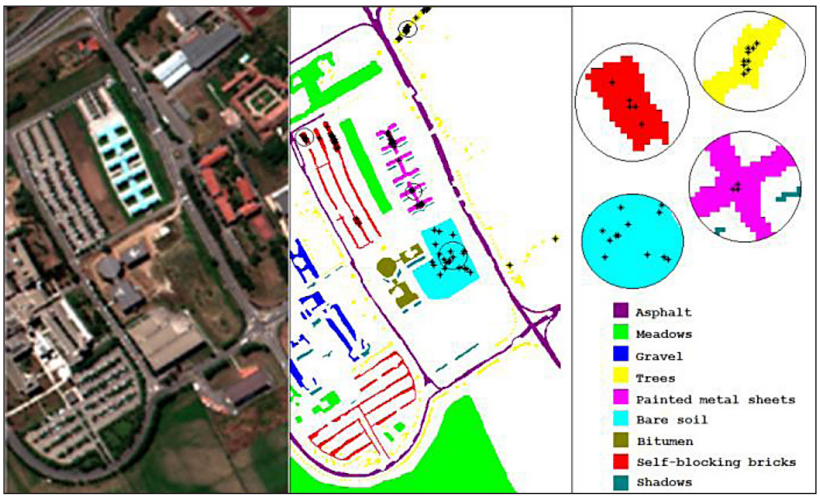

Fig. 2. False color composite of the Pavia University data set (a); Nine ground-truth classes of the Pavia University data set and chosen pixels for four endmembers (b)

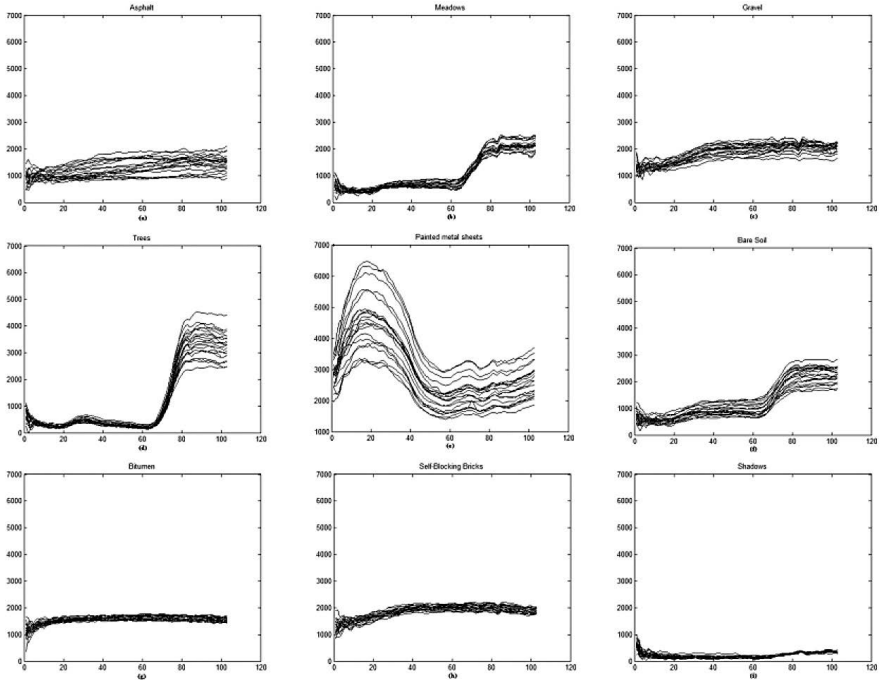

Fig. 3. Samples from Pavia University data set: (a) asphalt, (b) meadows, (c) gravel, (d) trees, (e) painted metal sheets, (f) bare soil, (g) bitumen, (h) self-blocking bricks, (i) shadows

Simulated data

Synthetic mixed pixels were generated by the combination of $M = 3$ multivariate Gaussian random endmembers.

Three high correlation endmembers, including asphalt, bitumen, and self-blocking bricks were selected from the Pavia University data-set. The correlation of endmembers ($\rho_{ij} = \frac{E\{\varepsilon_i^T \varepsilon_j\}}{\sqrt{E\{\varepsilon_i^T \varepsilon_i\}}\sqrt{E\{\varepsilon_j^T \varepsilon_j\}}}$) was used as a measure of dependence between endmembers. The correlation matrix of these endmembers was: $\rho = \begin{bmatrix} 1.000 & 0.994 & 0.997 \\ 0.994 & 1 & 0.998 \\ 0.997 & 0.998 & 1 \end{bmatrix}$.

Random samples from endmembers were selected to create synthetic mixtures with random abundances. Abundances were simulated from a uniform distribution over the set of proportion values that satisfy the non-negativity and sum-to-one constraints. The accuracy of the proposed unmixing algorithm was tested on the 100 synthetic mixed pixels created using the above procedure. First the MSOM transformation was computed using the endmember mean vectors. The endmembers and mixed pixels were transformed into a new MSOM space with dimension 3 (number of endmembers). Unmixing was done in this space using the described gradient descent algorithm. The starting point for gradient descent optimization was computed using FCLS unmixing in the original space.

For comparison the MESMA, Bayesian NCM [10], and ED algorithms [26] were run on the above synthetic mixed pixels.

The Bayesian NCM algorithm assumes that the covariance matrix of the endmembers in the NCM model is proportional to the identity matrix. This algorithm estimates abundances in a hierarchical Bayesian framework and uses a Markov Chain Monte Carlo sampling approach for estimating abundance fractions. In our experiments, 5000 iterations were used for sampling.

Prior to running the ED algorithm, data dimensionality was reduced from 113 bands to M dimensions using principal component analysis (PCA). The polynomial prior was used as the prior on the abundance vectors:

$$f(f_i) = \frac{1}{Z}\left(\sum_{m=1}^{M} b_m + 1 - \sum_{m=1}^{M} b_m (f_{mi} - c_m)^2\right) \quad (35)$$

where: Z – is a normalization constant given by

$$Z = \frac{\sqrt{M}\left(\sum_{m=1}^{M} b_m + 1\right)}{(M-1)!} - \sqrt{M}\sum_{m=1}^{M}\frac{b_m}{(M-1)!}\left(\left(c_m - \frac{1}{M}\right)^2 + \frac{M-1}{(M+1)M^2}\right). \quad (36)$$

The f and c vectors are constrained to abundance non-negativity and sum-to-one constraints. The b_m terms control the steepness of the prior. For more details see [26]. The value $b_m = 0.1$ is used in this implementation. The starting point for nonlinear optimization was computed using least square unmixing in the original space.

For a comparison of algorithms, the mean squared abundance residual errors of the mixed pixels were used as a measure. In addition, we also provide significance level analysis of abundance estimation results based on a paired-samples T-test. The results, as illustrated in Table 1, show that the proposed algorithm performs better than the other unmixing algorithms. The high correlation among endmembers prevented the separation of these endmembers in the MESMA, Bayesian NCM, and ED algorithms.

Table 1. Average squared abundance residual errors of four algorithms in the first experiment and p-value obtained by conducting paired-samples T-test between proposed algorithm and the other algorithms

Algorithm	Abundance Estimation Error	P-value
MESMA	0.297	0.112
Bayesian NCM	0.302	0.049
ED	0.321	0.041
Proposed algorithm	0.260	–

As mentioned above M principal components were used in the ED algorithm. The ED error can be decreased using a larger number of principal components. For example, using $2M$ principal components, the error was decreased to 0.301, and using $3M$ principal components, the error was decreased to 0.299.

Real hyperspectral image

In order to demonstrate the operational potential of the proposed algorithm, a sub 16×36 image of the Pavia University image was selected and unmixed by the proposed algorithm. Figure 4a shows a false color composite of this image, while Figure 4b shows the ground-truth of the image. About 29% of the pixels in the image have ground truth information. The ground truth image shows that the image contains spectra from trees, asphalt, and self-blocking bricks. Also, as can be seen, there were some shadow pixels near trees. The shadow pixels had no ground truth information.

Four endmembers including asphalt, trees, self-blocking bricks, and shadows were selected

a) b)

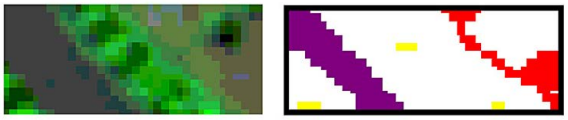

Fig. 4. False color composite of the pavia subscene (a); ground-truth classes of the subscene (b)

and four algorithms including MESMA, Bayesian NCM, ED, and proposed algorithms were run to generate proportion maps. The correlation matrix of these endmembers was:

$$\rho = \begin{bmatrix} 1.000 & 0.739 & 0.997 & 0.924 \\ 0.739 & 1.000 & 0.693 & 0.829 \\ 0.997 & 0.693 & 1.000 & 0.904 \\ 0.924 & 0.829 & 0.904 & 1.000 \end{bmatrix}.$$

Figure 5 illustrates generated proportion maps. Ideal abundances for labeled pixels were considered, such that pixels of each class were considered pure pixels of corresponding endmembers. Ideal proportion maps of the labeled pixels were illustrated in the first row of Figure 5.

The mean squared abundance residual errors of the labeled pixels were used as a measure of unmixing accuracy. The results, as illustrated in Table 2, show that the proposed algorithm performs significantly better than the other unmixing algorithms, and better agrees with the ground truth information.

By examining the abundance maps generated by the four algorithms, it can be seen that all algorithms are able to generate relatively good abundance maps for tree endmember. All algorithms had a small response over tree pixels in the other endmembers.

Table 2. Average squared abundance residual errors of four algorithms for pavia sub image and p-value obtained by conducting paired-samples T-test between proposed algorithm and the other algorithms

Algorithm	Abundance Estimation Error	P-value
MESMA	0.281	<0.001
Bayesian NCM	0.133	0.010
ED	0.128	0.024
Proposed algorithm	0.078	–

We considered the asphalt ground truth class. Examining the abundance map generated by the MESMA, Bayesian NCM, and ED algorithms, illustrates that many pixels other than asphalt have nonzero abundance values associated with asphalt's endmember. In contrast, in the abundance map generated by the proposed algorithm, very few pixels other than asphalt have a nonzero abundance value associated with asphalt's endmember. Furthermore, asphalt pixels have larger abundance values associated with the asphalt endmember in the proposed algorithm's results.

Examining the abundance map generated by the MESMA, Bayesian NCM, and ED algorithms shows that the three methods had some response over the asphalt regions in the self-blocking bricks and shadow proportion maps. However, in

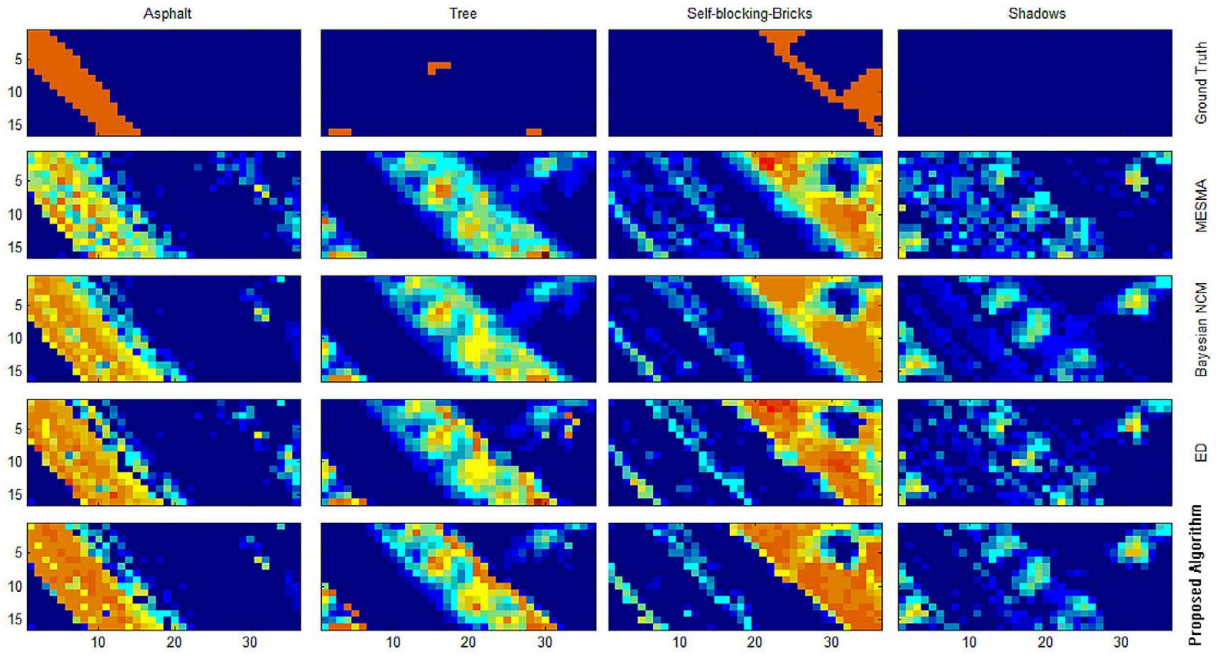

Fig. 5. The ground truth (first row) and proportion maps of the pavia subimage from MESMA (secound row), Bayesian NCM (third row), ED (fourth row) and proposed (fifth row)

the proposed algorithm, the number of such pixels is very low.

Three endmembers including asphalt, self-blocking bricks, and shadows were very similar to each other. The high correlation among these endmembers prevented the separation of these endmembers in the MESMA, Bayesian NCM, and ED algorithms.

Results on the Aviris Indian Pines data

The proposed algorithm was also run on simulated and real hyperspectral data using the June 1992 Aviris data set collected over the Indian Pines test site in Northwestern Indiana. The indian pines data-set consists of pixels and 224 spectral reflectance bands in the wavelength range 0.4 to 2.5 μm. We have also reduced the number of bands to 200 by removing bands covering the region of water absorption. This data-set contains two-thirds agriculture, and one-third forest or other natural perennial vegetation. Since the scene is taken in June some of the crops present, corn, soybeans, are in early stages of growth with residue from the previous crop. There is ground truth data for this image. Sixteen land-cover classes were identified in the Indian Pines scene: alfalfa, corn-notill, corn-mintill, corn, grass-pasture, grass-trees, grass-pasture-mowed, hay-windrowed, oats, soybean-notill, soybean-mintill, soybean-clean, wheat, woods, buildings-grass-trees-drives, and stone-steel-towers. Figure 6a shows band 29 of the dataset, while Figure 6b shows the ground-truth classes of interest. The no till, min till, and clean till labels indicate the amount of previous crop residue remaining. No till corresponds to a large amount of residue, min till has a moderate amount, and clean till has a minimal amount of residue [26].

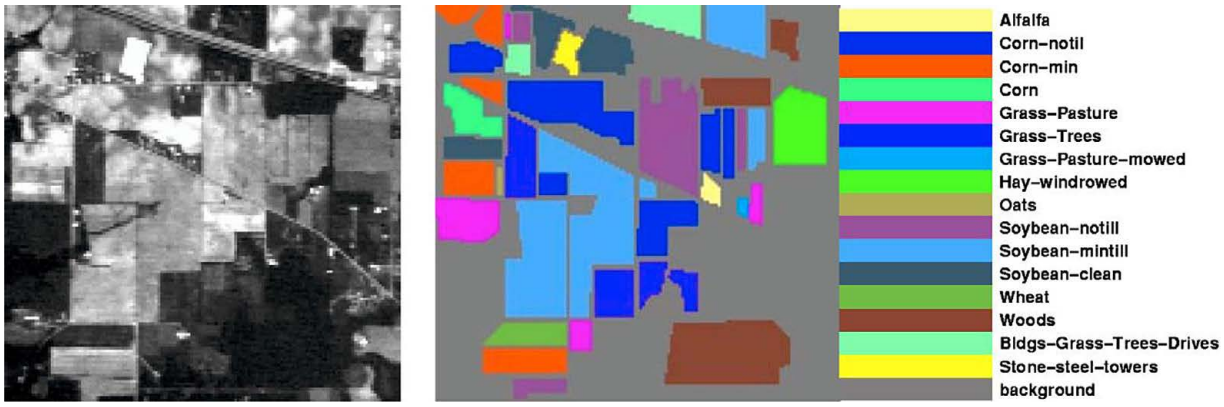

Fig. 6. Indian Pines scene (a); Sixteen ground-truth classes of the Indian Pines data set (b)

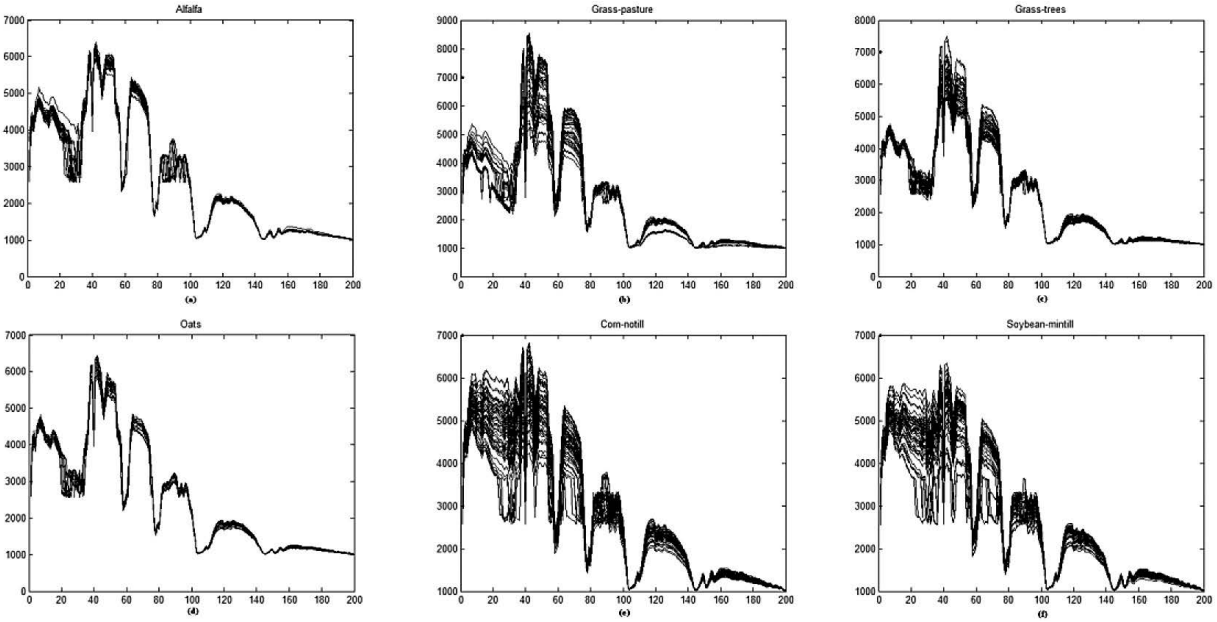

Fig. 7. Samples from Indian Pine data set. (a) alfaalfa, (b) grass-pasture, (c) grass-tree, (d) oats (e) corn-notil, (f) soybean-mintil

The sample mean and sample covariance of twenty samples of each class were used for the determination of the multivariate Gaussian random endmember mean and covariance matrices. Some of the endmember samples are shown in Figure 7.

Simulated data

Synthetic mixed pixels were generated by the combination of $M = 4$ multivariate Gaussian random endmembers. Four endmembers including corn-notill, grass-pasture, alfalfa, and oats were selected from Indian Pines data-set. The correlation matrix of these endmembers was:

$$\rho = \begin{bmatrix} 1.000 & 0.968 & 0.990 & 0.987 \\ 0.968 & 1.000 & 0.991 & 0.993 \\ 0.990 & 0.991 & 1.000 & 0.997 \\ 0.987 & 0.993 & 0.997 & 1.000 \end{bmatrix}.$$

The accuracy of the proposed unmixing algorithm was tested on the 100 synthetic mixed pixels. For comparison, MESMA, Bayesian NCM [10], and ED algorithms [26] were run on the above synthetic mixed pixels. For a comparison of algorithms, the mean squared abundance residual errors of the mixed pixels were used as a measure. The results, as illustrated in Table III, show that the proposed algorithm performs better than the other unmixing algorithms.

Table 3. Average squared abundance residual errors of four algorithms for simulated Indian Pine pixels and p-value obtained by conducting paired-samples T-test between proposed algorithm and the other algorithms

Algorithm	Abundance Estimation Error	P-value
MESMA	0.207	0.112
Bayesian NCM	0.336	<0.001
ED	0.201	0.129
Proposed algorithm	0.196	–

As mentioned above, $M=4$ principal components were used in the ED algorithm. The ED error can be decreased using a larger number of principal components. For example using $2M$ principal components was decreased the error to 0.20, and using $3M$ principal components was decreased the error to 0.199.

Real Hyperspectral Image

In order to demonstrate the operational potential of the proposed algorithm, a sub image of Indian Pines image was selected and unmixed by the proposed algorithm. Figure 8a shows a false color composite of this image, while Figure 8b shows the ground-truth of image. The ground truth image shows that the image contains spectra from corn-notil, grass-tree, and soybean-mintil.

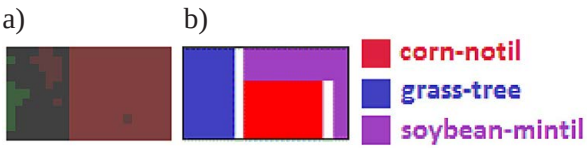

Fig. 8. False color composite of the Indian Pines subscene (a); Ground-truth classes of the subscene (b)

Three endmembers including corn-notil, grass-tree, and soybean-mintil were selected and four algorithms including MESMA, Bayesian NCM, ED, and proposed algorithms were run to generate proportion maps. The correlation matrix of these endmembers was:

$$\rho = \begin{bmatrix} 1.000 & 0.984 & 0.999 \\ 0.984 & 1.000 & 0.984 \\ 0.999 & 0.984 & 1.000 \end{bmatrix}.$$

Figure 9 illustrates generated proportion maps. Ideal abundances for labeled pixels were considered, such that pixels of each class were considered pure pixels of corresponding endmembers. Ideal proportion maps of the labeled pixels were illustrated in the first row of Figure 9. The mean squared abundance residual errors of the labeled pixels were used as a measure of unmixing accuracy. The results, as illustrated in Table 4, show that the proposed algorithm performs significantly better than the other unmixing algorithms and better agrees with the ground truth information.

Table 4. Average squared abundance residual errors of four algorithms for the Indian Pine sub image and p-value obtained by conducting paired-samples T-test between proposed algorithm and the other algorithms

Algorithm	Abundance Estimation Error	P-value
MESMA	0.394	<0.001
Bayesian NCM	0.368	0.032
ED	0.341	0.045
Proposed algorithm	0.295	–

By examining the abundance maps generated by the four algorithms, it can be seen that all algorithms are able to generate relatively good abundance maps for grass-tree endmember. All algorithms had a small response over grass-tree pixels in the other endmembers.

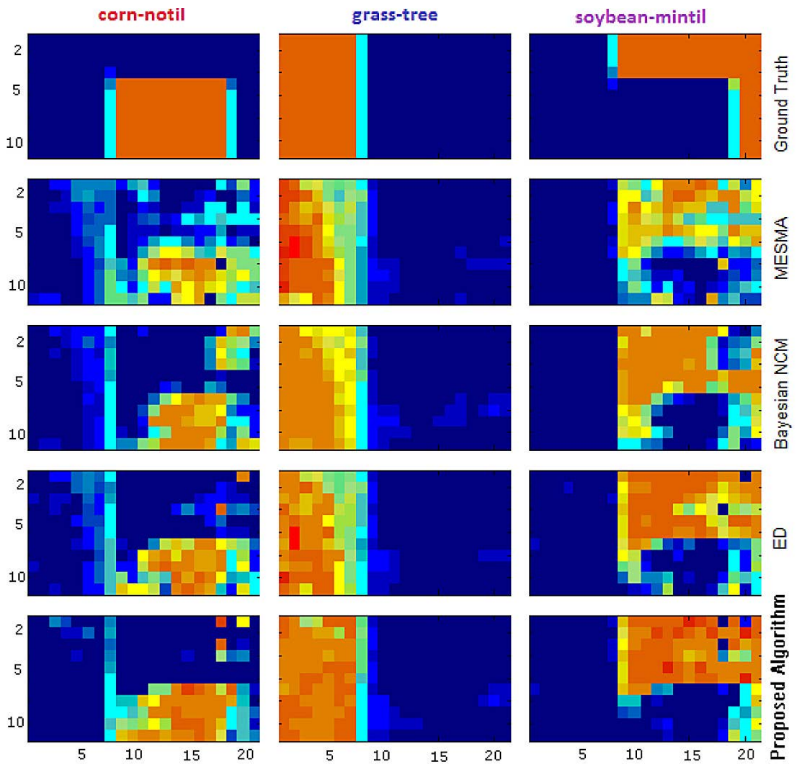

Fig. 9. The ground truth (first row) and proportion maps of the Indian Pines subimage from MESMA (secound row), Bayesian NCM (third row), ED (fourth row) and proposed algorithm (fifth row)

We considered the corn-notil ground truth class. Examining the abundance map generated by the MESMA, Bayesian NCM, and ED algorithms, illustrates that many pixels other than corn-notil have nonzero abundance values associated with corn-notil's endmember. In contrast, in the abundance map generated by the proposed algorithm, very few pixels other than corn-notil have a nonzero abundance value associated with corn-notil's endmember. Furthermore, corn-notil pixels have larger abundance values associated with the corn-notil endmember in the proposed algorithm's results.

Examining the abundance map generated by the MESMA, Bayesian NCM, and ED algorithms shows that the three methods had some response over the grass-tree regions in the soybean-mintil proportion maps. However, in the proposed algorithm, the number of such pixels is very low.

The high correlation between corn-notil and soybeans-mintil prevented the separation of these endmembers in the MESMA, Bayesian NCM, and ED algorithms.

CONCLUSIONS

Statistical distribution of endmembers in SMM must be selected carefully in order to have two important properties. First, this endmember representation must cover all possible spectra for the corresponding material. Second, this representation must not allow endmember variations that are not physically meaningful. Currently, there is no published theory for selecting the right distribution for endmembers.

In this paper, we have presented an algorithm for hyperspectral unmixing considering endmember variability. This algorithm uses MSOM linear transformation to orthonormalize the endmember mean vectors and reduce the dimension. Thus in the MSOM space, each feature is the linear combination of L original space features. According to the central limit theorem, with the large number of bands in the hyperspectral images, we can assume a Gaussian distribution for a weighted linear combination of endmember bands. Thus NCM is an appropriate choice in the MSOM space. Thus in this space, the endmembers are represented by correlated Gaussian random vectors with full correlated covariance matrices.

In the MSOM space, endmember means are orthonormal to each other. Due to high spectral angle between similar endmembers, the MSOM space has improved discrimination. Thus, in this space, the unmixing error is smaller. Moreover, the MSOM method reduces dimension to the

number of endmembers (*M*). In contrast to other dimension reduction methods that require a parameter to determine the number of dimensions, this method does not have any parameters. Furthermore, in the new lower dimensional space the endmember matrix is square, making it more appropriate than the non-square matrices of other methods.

The proposed algorithm was shown to be able to successfully perform unmixing on both simulated data and real hyperspectral imagery. The proposed algorithm was compared with three other abundance estimation methods, (MESMA, Bayesian NCM, and ED) using simulated and real hyperspectral data. The experimental results showed that the proposed algorithm performs better than the other unmixing algorithms.

REFERENCES

1. Jin J., Wang B., Zhang L. A novel approach based on fisher discriminant null space for decomposition of mixed pixels in hyperspectral imagery. Geoscience and Remote Sensing Letters, IEEE, 7(4), 2010, 699–703.
2. Chang C.I. An information-theoretic approach to spectral variability, similarity, and discrimination for hyperspectral image analysis. Information Theory, IEEE Transactions on 46(5), 2000, 1927–32.
3. Nascimento J.M., Dias J.M. Does independent component analysis play a role in unmixing hyperspectral data? Geoscience and Remote Sensing, IEEE Transactions on 43(1), 2005, 175–187.
4. Zhang B., Zhuang L., Gao L., Luo W., Ran Q., Du Q. PSO-EM: A hyperspectral unmixing algorithm based on normal compositional model. Geoscience and Remote Sensing, IEEE Transactions on 52(12), 2014, 7782–7792.
5. Bioucas-Dias J.M., Plaza A., Dobigeon N., Parente M., Du Q., Gader P., Chanussot J. Hyperspectral unmixing overview: Geometrical, statistical, and sparse regression-based approaches. Selected Topics in Applied Earth Observations and Remote Sensing, IEEE Journal of 5(2), 2012, 354–379.
6. Keshava N., Mustard J.F. Spectral unmixing. Signal Processing Magazine, IEEE 19(1), 2002, 44–57.
7. Bishop C.M. Pattern recognition and machine learning. Springer, 2006.
8. Cho M.A., Mathieu R., Debba P. Multiple endmember spectral-angle-mapper (SAM) analysis improves discrimination of savanna tree species. In: Hyperspectral Image and Signal Processing, Evolution in Remote Sensing, WHISPERS'09. IEEE First Workshop on, 2009, 1–4.
9. Dobigeon N., Tourneret J.Y., Chang C.I. Semi-supervised linear spectral unmixing using a hierarchical Bayesian model for hyperspectral imagery. Signal Processing, IEEE Transactions on 56(7), 2008, 2684–2695.
10. Eches O., Dobigeon N., Mailhes C., Tourneret J.Y. Bayesian estimation of linear mixtures using the normal compositional model. Application to hyperspectral imagery. Image Processing, IEEE Transactions on 19(6), 2010, 1403–1413.
11. Eches O., Dobigeon N., Tourneret J.Y. Estimating the number of endmembers in hyperspectral images using the normal compositional model and a hierarchical Bayesian algorithm. Selected Topics in Signal Processing, IEEE Journal of 4(3), 2010, 582–591.
12. Eismann M.T., Stein D. Stochastic mixture modeling. Hyperspectral Data Exploitation: Theory and Applications, 2007, pp. 148.
13. Ejaz M. A framework for implementing independent component analysis algorithms. ProQuest, 2008.
14. Hyvärinen A., Karhunen J., Oja E. Independent component analysis. John Wiley & Sons, 2004.
15. Kazianka H. Objective Bayesian analysis for the normal compositional model. Computational Statistics & Data Analysis, 56(6), 2012, 1528–1544.
16. Mei S., He M., Wang Z., Feng D. Spatial purity based endmember extraction for spectral mixture analysis. Geoscience and Remote Sensing, IEEE Transactions on 48(9), 2010, 3434–3445.
17. Padma S., Sanjeevi S. Jeffries Matusita based mixed-measure for improved spectral matching in hyperspectral image analysis. International Journal of Applied Earth Observation and Geoinformation 32, 2014, 138–151.
18. Roberts D.A., Gardner M., Church R., Ustin S., Scheer G., Green R.O. Mapping chaparral in the Santa Monica Mountains using multiple endmember spectral mixture models. Remote Sensing of Environment 65(3), 1998, 267–279.
19. Shao Z., Zhang L. Sparse dimensionality reduction of hyperspectral image based on semi-supervised local Fisher discriminant analysis. International Journal of Applied Earth Observation and Geoinformation 31, 2014, 122–129.
20. Somers B., Asner G.P., Tits L., Coppin P. Endmember variability in spectral mixture analysis: A review. Remote Sensing of Environment 115(7), 2011, 1603–1616.
21. Somers B., Zortea M., Plaza A., Asner G.P. Automated extraction of image-based endmember bundles for improved spectral unmixing. Selected Topics in Applied Earth Observations and Remote Sensing, IEEE Journal of 5(2), 2012, 396–408.
22. Stein D. Application of the normal compositional

model to the analysis of hyperspectral imagery. Advances in Techniques for Analysis of Remotely Sensed Data, IEEE Workshop on 2003, 44–51.

23. Tits L., De Keersmaecker W., Somers B., Asner G.P., Farifteh J., Coppin P. Hyperspectral shape-based unmixing to improve intra-and interclass variability for forest and agro-ecosystem monitoring. ISPRS Journal of Photogrammetry and Remote Sensing 74, 2012, 163–174.
24. Van der Meer F.D., Jia X. Collinearity and orthogonality of endmembers in linear spectral unmixing. International Journal of Applied Earth Observation and Geoinformation 18, 2012, 491–503.
25. Vaiphasa C., Skidmore A.K., de Boer W.F., Vaiphasa T. A hyperspectral band selector for plant species discrimination. ISPRS Journal of Photogrammetry and Remote Sensing 62(3), 2007, 225–235.
26. Zare A., Gader P. PCE: Piecewise convex endmember detection. Geoscience and Remote Sensing, IEEE Transactions on 48(6), 2010, 2620–2632.
27. Zare A., Gader P., Casella G. Sampling piecewise convex unmixing and endmember extraction. Geoscience and Remote Sensing, IEEE Transactions on 51(3), 2013, 1655–1665.
28. Zare A., Ho K.C. Endmember variability in hyperspectral analysis: Addressing spectral variability during spectral unmixing. Signal Processing Magazine, IEEE 1(1), 2014, 95–104.